

HIGH-MASS PROTO-STELLAR CANDIDATES - I : THE SAMPLE AND INITIAL RESULTS

T.K.SRIDHARAN
tksriddha@cfa.harvard.edu

Harvard-Smithsonian Center for Astrophysics, 60 Garden Street, MS 78, Cambridge, MA 02138, USA.

H. BEUTHER, P. SCHILKE, K.M. MENTEN
beuther@mpifr-bonn.mpg.de, schilke@mpifr-bonn.mpg.de, kmenten@mpifr-bonn.mpg.de
Max-Planck-Institut für Radioastronomie, Auf dem Hügel 69, 53121 Bonn, Germany

F. WYROWSKI
wyrowski@astro.umd.edu

Department of Astronomy, University of Maryland, College Park, USA
Version from November 3, 2018

ABSTRACT

We describe a systematic program aimed at identifying and characterizing candidate high-mass proto-stellar objects (HMPOs). Our candidate sample consists of 69 objects selected by criteria based on those established by Ramesh & Sridharan (1997) using far-infrared, radio-continuum and molecular line data. Infrared-Astronomical-Satellite (*IRAS*) and Midcourse-Space-Experiment (*MSX*) data were used to study the larger scale environments of the candidate sources and to determine their total luminosities and dust temperatures.

To derive the physical and chemical properties of our target regions, we observed continuum and spectral line radiation at millimeter and radio wavelengths. We imaged the free-free and dust continuum emission at wavelengths of 3.6 cm and 1.2 mm, respectively, searched for H₂O and CH₃OH maser emission and observed the CO $J = 2 \rightarrow 1$ and several NH₃ lines toward all sources in our sample. Other molecular tracers were observed in a subsample.

While dust continuum emission was detected in all sources, most of them show only weak or no emission at 3.6 cm. Where detected, the cm emission is frequently found to be offset from the mm emission, indicating that the free-free and dust emissions arise from different subsources possibly belonging to the same (proto)cluster. A comparison of the luminosities derived from the cm emission with bolometric luminosities calculated from the *IRAS* far-infrared fluxes shows that the cm emission very likely traces the most massive source, whereas the whole cluster contributes to the far-infrared luminosity. Estimates of the accretion luminosity indicate that a significant fraction of the bolometric luminosity is still due to accretion processes. The earliest stages of HMPO evolution we seek to identify are represented by dust cores without radio emission.

Line wings due to outflow activity are nearly omnipresent in the CO observations, and the molecular line data indicate the presence of hot cores for several sources, where the abundances of various molecular species are elevated due to evaporation of icy grain mantles. Kinetic gas temperatures of 40 sources are derived from NH₃ (1,1) and (2,2) data, and we compare the results with the dust temperatures obtained from the *IRAS* data.

Comparing the amount of dust, and hence the gas, associated with the HMPOs and with ultracompact HII regions (UCHIIs) we find that the two types of sources are clearly separated in mass-luminosity diagrams: for the same dust masses the UCHII regions have higher bolometric luminosities than HMPOs. We suggest that this is an evolutionary trend with the HMPOs being younger and reprocessing less (stellar) radiation in the IR than the more evolved UCHII regions.

These results indicate that a substantial fraction of our sample harbors HMPOs in a pre-UCHII region phase, the earliest known stage in the high-mass star formation process.

Subject headings: stars:formation – stars: massive – ISM: hot-cores

1. INTRODUCTION

High-mass stars exert a decisive influence on the appearance and evolution of galaxies. Throughout their life cycle, they inject significant amounts of energy and momentum into their environments through stellar winds, molecular outflows, ultraviolet (UV) radiation and eventually supernova explosions. They also influence the formation of nearby low-mass stars, most of which are formed in dense clusters heavily affected by a few massive stars, the Trapezium cluster in Orion being a well studied nearby

example (Hillenbrand & Hartmann 1998). Clearly, questions concerning the number, birth-rates, distribution, and evolutionary timescales of massive stars are of critical importance for building a general picture of Galactic evolution, in addition to their being interesting in themselves. While a scenario exists for the formation of low mass stars, much less is known about the processes involved in the formation of high-mass stars, which we take to be stars with $M \geq 8M_{\odot}$ (corresponding to stars of spectral type earlier than B2) not having an optically visible pre-main-sequence

phase (Palla & Stahler 1993). This lack of knowledge is due to the fact that it is difficult to identify the earliest stages of the high-mass star formation process. Owing to their smaller numbers and shorter evolutionary timescales, high-mass star-forming regions are on the average more distant than low mass star-forming regions. Additionally, the clustered mode in which massive star formation generally seems to proceed makes it very difficult to resolve and locate young high-mass protostars, which are deeply embedded and usually show little or no near-infrared emission (see Menten & Reid 1995 for the case of the BN/KL region in Orion).

Recently, much attention has been dedicated to studies of massive star formation and significant progress is being made. A handful of sources likely to be young high-mass stellar objects have been identified. Among the best examples are G31.41+0.31mm (Cesaroni et al. 1994), G192.16 (Shepherd et al. 1998), *IRAS* 20126+4104 (Cesaroni et al. 1997), *IRAS* 23385+6053 (Molinari et al. 1998b) and G34.24+0.13mm (Hunter 1998). These objects are characterized by high luminosities ($> 10^4 L_{\odot}$), dense ($> 10^6 \text{ cm}^{-3}$) and warm ($> 100 \text{ K}$) molecular gas and strong dust emission. Since they only show very weak or no free-free emission at cm wavelengths from ionized gas, they have not yet developed an ultracompact HII (UCHII) region. Henceforth, we will call these objects in a pre-UCHII region phase high-mass proto-stellar objects, HMPOs for short. In this sense internally heated hot cores are a sub-class of HMPOs shortly before ultracompact HII regions become detectable.

The first cases of known HMPOs are in the vicinity of UCHII regions, a selection effect because they were mostly discovered during molecular line and/or dust continuum studies of the UCHII regions. However, the nearness of an UCHII region (i.e. within, say, less than 0.1 pc or a few arcsec in angular units) is obviously a draw-back if one wants to study the earliest and unimpaired stages of massive star formation: the physical and chemical conditions in the vicinity of the HMPOs are significantly modified by interactions with the UCHII regions and their precursors. Also, frequently it is observationally difficult to discriminate between material associated with the UCHII region and the nearby HMPO. The latter point can be partially resolved by high resolution and high dynamic range interferometric observations, which in some of the cases cited above have led to the detection of HMPOs in the same fields as the UCHII regions.

Systematic studies of a substantial sample of isolated HMPOs are highly desirable and samples of HMPO candidates have been investigated, e.g. by Molinari et al. (1996) and Henning et al. (2000). Here we describe a program of extensive observations of a new sample of candidate HMPOs and present results indicating that some of the sources studied are objects in the earliest evolutionary stage known so far. Progress reports on this project were presented earlier by Menten et al. (1999), Sridharan et al. (1999) and Beuther et al. (2000).

2. THE SAMPLE

We have selected a sample of candidate HMPOs based on the criteria discussed by Ramesh & Sridharan (1997). They studied the reliability of the criteria defined by Wood

& Churchwell (1989a) for identifying UCHII regions by their far-infrared properties and obtained a sample of relatively isolated HMPO candidates in the process. The objects are chosen from the *IRAS* Point Source Catalog and

- are detected in the high density gas tracing CS $J = 2 \rightarrow 1$ survey of massive star forming regions (Bronfman et al. 1996). These sources satisfy the criteria used by Wood & Churchwell (1989) to select UCHII regions by their FIR colors.
- are bright at FIR wavelengths ($F_{60} > 90 \text{ Jy} \wedge F_{100} > 500 \text{ Jy}$),
- are not detected in the Galaxy-wide (single dish) 5 GHz 1987 Green Bank (Gregory & Condon 1991) and Parkes-MIT-NRAO radio continuum surveys (Griffith et al. 1994; Wright et al. 1994) at flux densities above 25 mJy,
- are north of -20° declination.

The first two of these criteria are based on the expectation that dense gas is present and HMPOs and UCHII regions should resemble each other with regard to their dust and gas temperatures and luminosities. The third criterion ensures that we are dealing with *isolated* HMPO candidates in the sense that they do not have UCHII regions or more evolved HII regions in their vicinity (within arcminutes, i.e. a few parsecs at the typical distances of a few kpc). Ramesh & Sridharan (1997) have shown that the surveys under consideration are sensitive enough to detect the radio continuum emission from typical UCHII regions throughout the Galaxy. The last criterium ensures the observability with the telescopes we are using.

These criteria led to the identification of 69 candidate objects with kinematic distances (Brand & Blitz 1993) derived from the CS velocities. For sources inside the solar circle, there are two solutions for the kinematic distance. This ambiguity can in some cases be resolved by other means (see below). The sample is listed in Table 1 with systemic velocities, kinematic distances, and luminosities and temperatures derived from the HIREs database (see §3.1.1). Molinari et al. (1996) used a different set of far-infrared selection criteria to identify possible HMPO candidates. Their and our sample have a total of 15 sources in common.

Figure 1 (a and b) present plots of the Galactic distribution and scale height for the whole sample. Sources without distance ambiguity are those in the outer Galaxy and those at the tangential points. Furthermore, we solved the distance ambiguity for a few more sources by other approaches: for sources with scale heights over 170 pc at the far distance [> 4 times the average Galactic scale height of UCHII regions, 37 pc (Bronfman et al. 2000)] the near distance was adopted (18151–1208, 18272–1217 and 18517+0437); we chose this scaleheight, because 166 pc is the largest offset from the Galactic plane for a source with known distance (05553+1631). For 19217+1651 the far distance was adopted, because the observed VLA-cm fluxes are not explicable by an implied low mass star if the near distance is chosen. For a few objects distances of associated sources were found in the literature (see Table 1).

We note that our selection criteria will certainly miss interesting classes of HMPOs. The first class we would miss are the HMPOs that are so young and cold that their SEDs peak longward of $\sim 200 \mu\text{m}$ and are extremely weak at near infrared-wavelengths, making them undetectable by *IRAS* at $25 \mu\text{m}$ and thus excluding them from our sample. For example, a $10^4 M_{\odot}$ core of mean density of $5 \times 10^5 \text{ cm}^{-3}$ and a temperature of 25 K, emitting as a blackbody at a distance of 5 kpc, produces a $25 \mu\text{m}$ flux density that is two orders of magnitude below the 0.5 Jy detection limit of *IRAS* at that wavelength. A prototype of such a cold, young object might be NGC 6334/I(NORTH) (Gezari 1982; Megeath & Tieftrunk 1999). The other missing group consists of sources with strongly associated, but not coincident, mid-infrared sources which increase the *IRAS* $12\mu\text{m}$ flux and decrease the $25\mu\text{m}/12\mu\text{m}$ flux ratio, thus excluding them from our sample (e.g. 23385+6053, Molinari et al. 1998a).

In this paper, the first of a series describing our HMPO survey, we give an overview of the overall characteristics of the sample, covering the mid-infrared (*IRAS* and MSX) and mm and cm continuum and spectral line observations. Spatial structures are discussed and we compare bolometric luminosities, gas masses and cm luminosities of our sample with those of the ultracompact HII regions. H_2O and CH_3OH maser observations as signposts of high-mass star formation are presented and we discuss spectral line observations of NH_3 , CO, CH_3CN , thermal CH_3OH , SiO and H^{13}CO^+ .

A more detailed analysis and discussion of the various datasets and follow-up observations on individual sources will be published in forthcoming papers.

3. OBSERVATIONS AND RESULTS

3.1. Archival data

3.1.1. The *IRAS-HIRES* database

The Infrared Astronomical Satellite (*IRAS*) performed an unbiased, sensitive all sky survey at 12, 25, 60 and $100 \mu\text{m}$. Advanced processing of the survey data using the Maximum Correlation Method resulted in HIRES (High RESolution Processing) images, which have a higher spatial resolution than the original *IRAS* dataset (Aumann et al. 1990). We obtained images for the whole sample from the Infrared Processing and Analysis Center (IPAC) at 12, 25, 60, and $100 \mu\text{m}$ using 20 iterations of the algorithm. Spatial resolutions are between $\approx 40''$ ($12 \mu\text{m}$) and $100''$ ($100 \mu\text{m}$). These are approximate values because the HIRES resolution varies around the sky. Detailed descriptions of HIRES can be found on the IPAC web-site¹.

In a majority of fields the $12 \mu\text{m}$ peak positions correspond well with the $100 \mu\text{m}$ peaks within the positional uncertainties (for an example see Fig. 2 bottom), but in 6 of the sources the $12 \mu\text{m}$ peaks are clearly offset by more than $1'$ from the $100 \mu\text{m}$ peaks (see Table 3 and example in Fig. 2 top). In some cases the $12 \mu\text{m}$ images are tracing more evolved IR sources in the vicinity of our targets (e.g. 05358+3543, Porras et al. 2000). In other cases the $12 \mu\text{m}$ peaks could be due to external heating of small grains (see discussion below). A number of sources are

resolved at the higher resolution of the $12 \mu\text{m}$ images but appear unresolved at $100 \mu\text{m}$ (e.g. 05553+1631, see Fig. 2 center). Thus, the fluxes in the different bands in the *IRAS* point source catalog do not necessarily correspond to the same objects. The real fraction of non-coinciding 100 and $12 \mu\text{m}$ sources might be even higher, because the spatial resolution, even of the HIRES images, is not very good. To improve on the Point Source Catalog data we obtained the fluxes around the main dust cores (Beuther et al. 2001) from the HIRES images and fitted two-component greybodies to these data (opacity corrected, modified blackbodies to fit also the 1.2 mm data, Beuther et al. 2001). A cold dust component fits the $60 \mu\text{m}$ and $100 \mu\text{m}$ data and a hot component fits the $12 \mu\text{m}$ and $25 \mu\text{m}$ data. These fits reproduce the HIRES data well (see Figure 3 for examples) for temperatures of the cold dust component T_{cd} around 50 K and hot component T_{hd} between 150 K and 200 K (Table 1). While the hot component might represent a more evolved and hot inner core, it could also be due to small non-thermally excited grains exposed to external UV heating as found for many other *IRAS* sources (Mathis 1990). The MSX data (see §4.1) support this interpretation for a fraction of sources for which the MSX- and mm positions do not coincide. Integrating the two-component fits gives estimates of the total luminosities of our objects (Table 1). We find total luminosities in the range $10^{3.5} - 10^6 L_{\odot}$, therefore we conclude that the embedded sources are high-mass objects with ZAMS masses $\gtrsim 8 M_{\odot}$ (spectral type earlier than B2). The ratio of the flux in the hot component to that in the cold component varies between 0.05 and 0.4 with an average value around 0.16. This shows that the main contribution to the total luminosity comes from the cold components.

3.1.2. The *Midcourse Space Experiment (MSX) Point Source Catalog*

MSX, a Ballistic Missile Defense Organization satellite, surveyed the whole Galactic plane ($b \pm 6^\circ$) in 6 bands centered at 4.29, 4.35, 8.28, 12.13, 14.65, and $21.34 \mu\text{m}$. The sensitivity in the $4 \mu\text{m}$ bands is between 10 and 30 Jy/beam, in the other bands the sensitivity is better, ranging between 0.1 and a few Jy/beam. With a spatial resolution of $18.3''$, positions in the Point Source Catalog are accurate to an rms of $4'' - 5''$, and the calibration errors are well within 13%. For a more detailed description see, e.g., Egan et al. (1998) and the MSX web -site².

The MSX Point Source Catalog lists sources in 62 out of our 69 fields (Table 1). In a few cases multiple sources are found and a total of 87 sources are found toward our target regions. Except for 18540+0220 and 23151+5912 no sources were detected in the $4 \mu\text{m}$ bands, while in the other bands almost all of the sources are detected. Comparing the fluxes in the $12 \mu\text{m}$ and $21 \mu\text{m}$ bands (nearest to the $12\mu\text{m}$ & $25\mu\text{m}$ *IRAS* bands) the flux ratio is between 0.1 and 0.5 in 63 MSX sources, between 0.6 and 0.8 in 4 sources and undefined in 20 because of non-detection in either of the two bands. The flux ratios between 0.1 and 0.5 are similar to the *IRAS* flux ratios. For the main cores the flux ratios do not vary between sources with or without cm detections, therefore the MSX fluxes alone do

¹ <http://www.ipac.caltech.edu/ipac/iras/iras.html>

² <http://www.ipac.caltech.edu/ipac/msx/msx.html>

not allow determinations of the evolutionary phase of a source. The four sources with ratios in excess of 0.5 are found at the edge or offset from the main core as seen in the mm continuum and are most likely hotter and more evolved sub-sources.

3.2. *New observations*

3.2.1. *1.2 mm dust continuum emission*

Dust emission produced by massive cores has been found and mapped in all the fields and a detailed analysis of this extensive database is presented in an accompanying paper (Beuther et al. 2001). For the present discussion we only use the core masses derived from the 1.2 mm data.

3.2.2. *3.6 cm continuum emission*

Because small HII regions are in general difficult to detect in most existing centimeter-wavelength single dish surveys of the Galactic plane, we used the Very Large Array (VLA)³ to search for weak free-free emission at 3.6 cm using the B array with a synthesized beam of $0.7''$ and a 1σ rms sensitivity of ~ 0.1 mJy. The observations were carried out on July 2, 1998. Each source was observed twice at widely different hour angles, for a total of 10 minutes in order to improve *uv*-coverage. Suitable phase calibrators were observed at intervals of approximately 30 minutes. The data were reduced using NRAO's AIPS software using standard procedures.

Radio emission from objects in the pre-UCHII phase might be caused by recently ignited massive protostars and/or jet phenomena (e.g. Hofner et al. 1999). Background contamination by extragalactic radio sources at a 1 mJy level is estimated to be extremely low at this frequencies (0.007 per arcmin², Fomalont et al. 1991). Other processes such as synchrotron emission (Reid et al. 1995) or stellar winds could be producing the observed emission which require spectral index information for further elucidation. About 10% of the sources originally observed by Wood & Churchwell (1989b) are optically thick at 2 cm, and a similar or even higher percentage – since in the early stages we expect to find hypercompact sources (≤ 2000 AU, Tieftrunk et al. 1997) – might be applicable for our detections. Sources without any cm emission could be even younger objects, where either no star has ignited or the ionized region is so young and small that the free-free emission is still confined and not detectable down to the mJy level (Churchwell 2000). The mm observations (Beuther et al. 2001) prove that our sample indeed consists of massive cores which should produce high-mass stars, assuming normal IMFs. Out of the 66 fields observed at 3.6 cm, 24 show no emission at the 1 mJy level, and 19 have weak emission with flux densities below 10 mJy, while 21 sources show emission between 10 and a few 100 mJy. For the remaining 2 fields the dynamic range of our snapshot data is not good enough to draw a firm conclusion. Observed flux densities are listed in Table 3. Typical ultracompact HII region fluxes at distances of a few kpc are between a few mJy and more than a Jy (Wood & Churchwell 1989b), which is far higher than the flux densities observed in a substantial fraction of our sample. But there are also a number of well known sources which

exhibit cm continuum emission at a level not detectable with our sensitivity. The W3(OH) Turner-Welch object (also known as W3(H₂O)) at a distance of 2.2 kpc has a cm flux of 1.1 mJy (Reid et al. 1995) due to synchrotron emission, which is similar to our detection limit, but other sources like source I in Orion KL (Menten & Reid 1995) or Cep A East (Garay et al. 1996) would show fluxes below 0.3 mJy if moved to a distance of 2 kpc, which is below our detection limit. Therefore it is likely that deeper images of our sample would reveal more cm sources. The fact that the sample contains sources at different stages of evolution makes it an ideal laboratory to explore the evolution of massive stars with a consistent database.

3.2.3. *Spectral line observations*

In order to understand the chemistry, kinematics and energetics of our target regions, we conducted a number of different spectral line observations from mm to cm wavelengths.

Millimeter observations: outflow and dense core tracers

The IRAM 30-m telescope was used (mainly in spring 1998, and for several periods of a few hours duration in spring 1999 and 2000) to obtain single point spectra for 36 sources in a number of tracers sensitive to the physical and chemical conditions expected near HMPOs: high temperatures and densities, elevated abundances of molecular species resulting from evaporation of icy grain mantles, and outflow activity. In most cases a number of lines could be observed simultaneously (see Table 2).

The observations were conducted in the wobblers switching mode, where the wobbling secondary reflector switched in azimuth between the ON and an OFF position with a switching amplitude of $180''$ and a frequency of 0.5 Hz. For the CO data the OFF position is generally not free of emission, which corrupts the spectra at velocities around the systemic velocity but in general does not affect spatially more confined broad line wings in which we are primarily interested. As backends, we used the facility autocorrelator and two 512 MHz filterbanks.

To complete the CO line wing/outflow single positions search we observed the rest of the sample in June 2000 at the CSO in the ¹²CO(2 → 1) line (see Table 2). These data were obtained in the position switching mode, where the OFF positions were determined using Galactic CO surveys (Sanders et al. 1986; Dame et al. 1987) and verified to be free of emission.

We found CO line wings tracing bipolar outflows in 58 out of 69 sources. Six sources showed no line wings, and for 5 sources the spectra are too confused by Galactic plane emission to allow a classification. Assuming that line wings are only detectable for outflow sources with an inclination angle of at least 10° to the plane of the sky, statistically 11% (in our case ≈ 8 sources) should show no wing emission although an outflow could be present. That would be consistent with outflows being present in all of our sources and strongly suggests that outflow activity is an ubiquitous phenomenon not only in low mass star-forming regions but

³ The VLA is operated by the National Radio Astronomy Observatory (NRAO) with Associated Universities, Inc., under cooperative agreement with the National Science Foundation (NSF).

also in regions of massive star formation. Previous investigations that obtained similar results are e.g. Shepherd et al. (1996); Henning et al. (2000); Zhang et al. (2001) (see also the review by Churchwell 2000).

SiO emission as another outflow tracer (e.g. Schilke et al. 1997) was detected in the 30-m observations toward 23 out of 36 sources with wing emission seen in most cases.

Thermal emission from CH₃OH and/or CH₃CN was detected in 19 out of the 30 sources implying that hot core activity is prevalent. H¹³CO⁺(1 → 0) emission was found in all 36 observed sources, most likely tracing structures similar to the dust cores. We mostly used *IRAS* coordinates as source locations because at the time of the observations improved positions from 1.2 mm observations were not yet available. In 8 fields the main mm peak is offset from the *IRAS* position by more than the 1.2 mm FWHM beamwidth of 11", which would have lowered the detection rates.

H₂O and CH₃OH masers

During 1998 February and November, we searched for maser emission in the 22 GHz H₂O (mean rms ≈ 0.4 Jy) and 6.7 GHz CH₃OH lines (mean rms ≈ 0.2 Jy) toward all of our target sources using the Effelsberg 100 m telescope (see Table 2). The calibration error is estimated to be around 20%.

Both maser searches had high detection rates: 29 H₂O (10 of them new detections) and 26 CH₃OH masers (5 new detections) were found; toward 19 sources both H₂O and CH₃OH masers were detected (see Fig. 5 for examples). The CH₃OH detection rate of our sample differs from that of UCHII regions: We find CH₃OH maser toward 38% of the sources in our sample while Walsh et al. (1998) quote a detection rate of 20% toward UCHII regions. In contrast, the detection rate of the H₂O masers toward the sources of our sample is only 42%, while Churchwell et al. (1990) detect H₂O masers toward 67% of 84 UCHII regions they surveyed with comparable flux limits.

In Figure 6, we present the source and maser distribution of our sample in a Wood & Churchwell (1989)-style color-color diagram. While H₂O and CH₃OH maser sources are found all over the diagram, combined clustering of both maser types is much more common in the top-right corner, corresponding to the coldest and hence presumably the least evolved sources, which makes sources with colors in that area the most promising HMPO candidates.

While methanol maser emission is always confined to less than 15 km s⁻¹ in total around the systemic velocity the water masers nearly always emit over a much wider range (up to 70 km s⁻¹). Just comparing the same velocity ranges both types mostly show emission features at different velocities, which strongly confirms earlier assumptions that these maser types are emitted in different regions of the star-forming core (Menten 1996). While the methanol masers are probably confined to the innermost part – the molecular envelope of a central star or possibly a disk – water maser emission could originate there as well, but the higher velocities point to different emission spots, most likely in outflows (e.g. Marti et al. 1999).

Follow-up interferometric observations with the VLA (H₂O) and the Australian Telescope Compact Array

(ATCA, CH₃OH) have been conducted and a detailed analysis and comparison of the data with the other datasets will be published soon.

NH₃ observations

To obtain estimates of the kinetic temperature, the 100-m telescope was used to observe the NH₃(*J, K*) = (1,1), (2,2) inversion lines in the entire sample (see Table 2). The (1,1) line was detected toward 59 sources, and for 40 sources the (2,2) line was found to be strong enough to allow a meaningful estimate of the gas temperature. The rotation temperatures listed in Table 1 were derived following Ungerechts et al. (1986); in the relevant temperature range around 20 K kinetic temperatures are only marginally higher (Danby et al. 1988). The average rotation temperature is 19 K with the notable exception of 18089-1732 for which we derive 38 K. Molinari et al. (1996) found a similar mean value of $T_{\text{kin}} \sim 22$ K in their sample of young massive objects, which is identical to the average rotation temperature Churchwell et al. (1990) found toward UCHII regions. Comparing the NH₃ derived temperatures with the dust temperatures (from HIREs, Table 1) it is evident that the derived dust temperatures are on the average ~ 20 K higher than the rotation temperatures. This difference reflects the fact that *IRAS* was not sensitive to temperatures lower than 30 K and therefore detected emission from warm dust inside the core. In contrast to that the (1,1) and (2,2) ammonia lines trace the cooler and more extended envelope and therefore result in lower temperatures. It is possible and likely that NH₃(4,4) observations will reveal higher temperatures due to a warm inner core.

The average intrinsic NH₃ line widths we find in our sample is 2.0 km s⁻¹, while the average value found toward a sample of molecular cores associated with UCHII regions is 3.1 km s⁻¹ (Churchwell et al. 1990). This indicates significantly less turbulence in the presumably younger HMPOs possibly because in this young sources there has been less input of mechanical energy yet, e.g. by outflows.

4. DISCUSSION

4.1. *Source Multiplicity*

Positional comparison between MSX-/mm sources (Beuther et al. 2001) and MSX-/cm sources (Table 3) reveal median separations of approximately 7" (between 1" and 30") in both cases. The positional accuracy of MSX is 4" – 5" (Egan et al. 1998), comparable to that of the mm data, while the the cm data are more accurate, at better than 1". While the offsets mentioned might be due to positional uncertainties in many cases, there remain significant numbers of fields where the offsets are larger than any observational error and therefore the different tracers depict different sources. MSX sources located at the edges of the cores observed at mm-wavelengths might either be reflection nebulae, i.e. reprocessed radiation from a deeply embedded source, or they could also be sources belonging to the same evolving cluster as the mm source, but in a more advanced stage of evolution. Even younger stages of evolution might even be undetectable at 12μm (see also §2).

In 29 out of 42 fields with cm detections, MSX-, mm- and cm-sources are found. In most of these cases it is difficult to draw firm conclusions as to whether the emission in the three wavelength regimes arises from the same or from different sources, because the spatial resolution is insufficient. For the regions showing extended cm emission (of size larger than a few arcsecs), in 5 out of 7 sources the MSX-source is found to be associated with the cm- rather than with the mm-source. While we are dealing with low-number statistics, different stages of evolution in the same cluster are the most probable cause. The more evolved and therefore hotter sources exciting an UCHII region are more likely to emit at 12 μm and thus be detectable by MSX than the colder and more deeply embedded mm sources.

Generally, sources showing cm emission are found to be associated with the mm cores (Beuther et al. 2001), but the cm peak is mostly offset from the mm peak (Table 3). The median offset between mm and cm sources is 11'' (between 2'' and 40''). Given the positional accuracies quoted above, these offsets are real and not due to pointing problems. Assuming the near distance for sources with distance ambiguities the median projected separation between mm and cm peaks is ≈ 0.1 pc. Thus, while the sources most likely belong to the same (proto)cluster, they are clearly different sub-sources. The cm sources are probably slightly older and more evolved, while the mm sources might represent the youngest objects or object groups in the fields. For the few sources which seem to be coincident possible projection effects have also to be considered.

4.2. Mass-luminosity relations

To understand mass and luminosity evolution in the massive star formation process, we compare the masses derived from the mm continuum data (Beuther et al. 2001) and luminosities from the HIREs-data of our sample with other classes of objects. Since we selected our sample to contain objects in a pre-UCHII region phase, natural reference objects are UCHII regions. For this purpose we use UCHII region data from Hunter (1997) and Hunter et al. (2000) and estimate masses from 350 μm images using the same assumptions as employed by us (Beuther et al. 2001) for our 1.2 mm data. For a few sources Hunter et al. also have 1.3 mm data, and the masses separately derived using only the 1.3mm fluxes and the 350 μm fluxes agree well with each other.

In Figure 4(a) we plot far-infrared luminosities versus core masses for HMPOs and UCHII regions. The two groups appear separated, with the UCHII regions having higher bolometric luminosities than the HMPOs for the same core masses. We interpret this as an evolutionary effect caused by the embedded cluster, which becomes more luminous at FIR wavelengths while they evolve and destroy the cores from which they were born. Another possible explanation for this trend would be that different massive star clusters differ in their initial mass function (IMF) and that sources with UCHII regions form more massive stars than HMPOs. We think this is unlikely, because Massey (1998) finds for more than 20 OB associations essentially a Salpeter IMF ($N \propto m^{-1.35}$) with little variation. Therefore, we argue that we are indeed observing an evolutionary effect and our sample is on the average younger than UCHII regions.

Monte Carlo simulations to derive expected cluster luminosities over a wide range of cluster masses were performed using the methods outlined in Walsh et al. (2001). As Initial Mass Functions we used a Salpeter IMF ($N \propto m^{-1.35}$) for sources above 1 M_{\odot} (Massey 1998) and a Scalo IMF ($N \propto m^{-0.83}$) for sources below 1 M_{\odot} . The upper end of the IMF is still under discussion and Casassus et al. (2000) propose a steepening there, but we work with the distribution found by Massey (1998), which is based on observations of more than 20 OB associations. A steeper IMF would flatten the top end of the derived cluster luminosity distribution slightly, but qualitatively the results stay similar. As mass-to-luminosity relation $L \propto m^{\beta}$ we use $\beta = 2.8$ for $m < 1$, $\beta = 4$ for $1 < m < 30$ and $\beta = 2$ for $m > 30$ (Massey 1998; Schatzman & Praderie 1993). To scale the cluster masses to the initial core masses we assumed a star formation efficiency of 30% (Lada 1993), and the results are shown in greyscale in Figure 4(a). The shaded area indicates where 90% of the star clusters are expected to be found. The large spread in luminosity with given mass can be explained by the strong power law dependence between mass and luminosity. Many low mass stars do not raise the luminosity of the the cluster much, but the formation of just 1 massive star increases the cluster luminosity over orders of magnitude. The upper cutoff at luminosities higher than $10^6 L_{\odot}$ occurs because of an artificial upper mass truncation in the simulated IMF at 100 M_{\odot} . The main conclusion we derive from these simulations is that many HMPOs are underluminous compared to the expected cluster luminosities. The UCHII region luminosities agree better, but the most massive UCHII regions are found to be underluminous again. Since we expect the same formation processes in both types of sources with the same underlying IMFs (as stated by Massey 1998), this strengthens our conclusion that the HMPOs are in a younger stage of evolution and have not yet reached their final cluster luminosity. The Figure suggests further that objects evolve from HMPOs to UCHII regions to clusters.

A further support of the youth of our sample is outlined in Figure 4(b), which presents the distance independent M/L ratio in a histogram. As already expected from Figure 4(a) the ratio M/L is lower on the average for UCHIIs (peak at 0.01) than for HMPOs (peak at 0.05). This again can be explained with the HMPOs being younger and therefore less luminous than the more evolved UCHII regions. A higher M/L ratio could also indicate sample of less massive stellar objects on an average, but this is not the case in our sample because the core mass ranges of the HMPOs and the UCHII regions are similar (see Fig. 4(a)).

4.3. Bolometric- versus cm luminosities

We calculate from the measured cm fluxes the expected stellar luminosities of the central sources [as outlined in Kurtz et al. (1994, eqs. 1 & 3) assuming the emission to be optically thin at 3.6 cm] and compare them to the IR luminosities obtained from the *IRAS* data base. For optically thick emission, which we expect in a fair number of our sources, the derived luminosities are lower limits. Figure 7 presents the derived cm luminosities plotted against the corresponding IR luminosities. It is obvious that the IR luminosities are on the average far higher than the cm luminosities; similar results were found by Testi (2000)

and Walsh et al. (2001) on different samples. This most likely reflects the fact that the cm data trace just one single already ignited star while the IR data – due to the large *IRAS* beam – are tracing a whole cluster with many sources, some younger with no H-burning at their center yet, and others too weak to ionize a significant UCHII region, which by now is the standard scenario. This would be consistent with massive stars forming only in clusters (Stahler et al. 2000). A possible caveat is that some of the young ultracompact or even hypercompact HII regions could be confined strongly and be optically thick which leads to an underestimate of the cm luminosities. Data at other wavelengths are necessary to define the spectral indices and by that the ratio of optically thick sources. Additionally, accretion contributions to the luminosities have to be taken into account (see §4.4). All these phenomena explain the observations qualitatively well, but separating the different contributions quantitatively is not possible with the present database.

4.4. Accretion luminosity

Luminosity due to accretion plays a significant role in the formation of massive stars. We assume a simplified relation for the accretion luminosity (Wolfire & Cassinelli 1987):

$$L_{\text{acc}} = \frac{GM_*\dot{M}}{R_*}$$

with G the gravitational constant, M_* the mass of the (proto)star, \dot{M} the accretion rate and R_* the stellar radius. Main sources of uncertainty are the accretion rate and the radius of the accreting star. Assuming an accretion rate of $\dot{M} = 10^{-3} M_{\odot}/\text{yr}$ (based on outflow observations of this sample presented in a forthcoming paper by Beuther et al., in prep.) the accretion luminosity for stars between 10 and 40 M_{\odot} is around $6 \times 10^4 L_{\odot}$. While the accretion rate we choose for this estimate is an upper limit in current theories of high-mass star formation (e.g. Bernasconi & Maeder 1996; Norberg & Maeder 2000; Osorio et al. 1999), the radius of the evolving protostar is expected to be larger than the final main sequence radius we employed (Bernasconi & Maeder 1996). Thus, these accretion luminosities are upper limits to true accretion luminosities. With this assumed accretion rates it takes 3×10^4 years to build a 30 M_{\odot} star which has a luminosity comparable to the accretion luminosity. Using the increasing accretion rates by Norberg & Maeder (2000) equality of stellar and accretion luminosities is reached even later, at times around 10^6 years. Osorio et al. (1999) find for a number of well known hot cores that accretion still produces around 90% of the bolometric luminosity after a few times 10^4 years. In the models of intermediate-mass stars by Palla & Stahler (1993) the radiative luminosity matches the accretion luminosity after around 10^5 years. While the time scales differ between the different models, in all the cases the accretion luminosity plays a dominant role for a significant amount of time during the massive cluster forming process. Now, comparing the accretion luminosities with the IR derived luminosities of our sample (Table 1) it seems very likely that in many objects a significant part of the detected flux is due to accretion. However, at this stage of the investigation we cannot determine what

fractions of the total luminosity are due to accretion and nuclear burning. High accretion rates (Norberg & Maeder 2000) would also cause quenching of the UCHII cm radiation in the initial stages of evolution (Walmsley 1995; Osorio et al. 1999), consistent with our low average cm fluxes.

5. CONCLUSIONS

Our selection criteria – basically CS detections of bright *IRAS* point sources with colors similar to ultracompact HII regions and the absence of significant free-free emission at 5 GHz – were very successful in finding sources at the earliest known stages of high-mass star formation. An analysis of the *IRAS*-HIRES and MSX-data gives an overview of spatial structures on large scales and the spectral energy distributions. We find bolometric luminosities of $10^4 - 10^6 L_{\odot}$ and dust temperatures around 40 K.

- VLA cm observations reveal that a large fraction of the sample does not emit free-free emission down to 1 mJy, which suggests that the sources are at very early evolutionary stages. The majority of the detected cm peaks is spatially offset from the mm peaks which implies different sources in different evolutionary stages being responsible for the different emission features.
- Luminosities based on the cm emission are on the average far lower than bolometric luminosities derived in the FIR. The most likely explanation for this phenomenon is that the cm emission traces just one massive star whereas the FIR-emission reflects the whole cluster luminosity. It has to be taken into account that the cm emission might still be optically thick in a number of sources, which results in an underestimation of the intrinsic luminosity.
- HMPOs are found to have a higher mass to luminosity ratio than UCHII regions. The most likely explanation is that the HMPOs are significantly younger with more molecular gas left and less (stellar) radiation reprocessed in the IR. Evolving further to the UCHII region stage the sources become more luminous and start destroying their surrounding gas cocoons.
- Comparing estimated accretion luminosities with the derived bolometric luminosities indicates that in many sources a large fraction of the total luminosity could be due to accretion processes.
- Outflow phenomena are ubiquitous and methanol and water maser detection rates are high. Other molecular species such as SiO (outflow tracer), H^{13}CO^+ (dense gas tracer) and hot core tracers like CH_3OH and CH_3CN were found in a large fraction of the observed sources.
- Rotation temperatures from NH_3 (1,1) and (2,2) lines in 40 out of 69 sources are on the average 20 K, about 20 K lower than the HIRES-derived dust temperatures. This phenomenon has been found frequently and comes about because *IRAS* was not

sensitive to temperatures below 30 K and observed warmer dust further inside the core. On the contrary, NH_3 (1,1) and (2,2) is sensitive to the cooler and more extended envelope, which results in lower temperatures.

We have carried out further single dish and interferometric studies of promising objects from this sample. These results will be published in forthcoming papers (Beuther et al. Wyrowski et al. in preparation). Combined with efforts by other groups a reasonable sized sample of HMPO candidates now exists, and in the near future a good observational characterization of HMPOs can be achieved to confront theories.

We are indebted to Andrew Walsh for the Monte Carlo simulations of the cluster luminosities. We thank Frank

Bertoldi, Malcolm Walmsley and Floris v.d. Tak for many useful comments on earlier versions of this paper. Additionally, we thank Eberhard Hansis who worked on the HIRES data and resolved some distance ambiguities. We also like to thank Frederique Motte, Bernd Weferling and again Frank Bertoldi, who conducted the bolometer observations at Pico Veleta. Last but not least, we thank the referee for additional improving comments. The observational work was conducted at the Effelsberg 100m, the VLA, the IRAM 30m and the CSO (supported by the NSF grant AST 96-15025). It has made extensive use of the IPAC and SIMBAD databases. H. Beuther gets support by the *Deutsche Forschungsgemeinschaft*, DFG project number SPP 471. F. Wyrowski is supported by the National Science Foundation under Grant No. AST-9981289.

REFERENCES

- Aumann H.H., Fowler J.W., Melnyk M., 1990, *AJ*, 99, 1674
 Bernasconi P.A., Maeder A., 1996, *A&A*, 307, 829
 Beuther H., Sridharan T.K., Schilke P., Wyrowski F., Menten K.M., 2000, in: *Star Formation from The Small to the Large Scale*, ESA SP-445
 Beuther H., Schilke P., Menten K.M., Sridharan T.K., Wyrowski F., Motte F., 2001, *ApJ*, submitted
 Blaauw A., 1964, *Annual Review of A&A*, p. 213
 Brand J., Blitz L., 1993, *A&A*, 275, 67
 Brand J., Cesaroni R., Caselli, P., et al. 1994, *A&AS*, 103, 541
 Bronfman L., Nyman L.A., May J., 1996, *A&AS*, 115, 81
 Bronfman L., Casassus S., May J., Nyman L.-A., 2000, *A&A*, 358, 521
 Caswell J.L., Vaile R.A., 1995, *MNRAS*, 273, 328
 Casoli F.; Combes F., Dupraz C., Gerin M., Boulanger F., 1986, *A&A*, 169, 281
 Casassus S., Bronfman L., May J., Nyman L.-A., 2000, *A&A*, 358, 514
 Cesaroni R., Churchwell, E., Hofner, P., Walmley, C.M., Kurtz, S., 1994a, *A&A*, 252, 278
 Cesaroni, R., Felli, M., Testi, L., Walmley, C.M., Olmi, L., 1997, *A&A* 325, 725
 Cesaroni R., Felli M., Jenness T., et al. 1999, *A&A*, 345, 949
 Churchwell E., Walmsley C., Cesaroni R., 1990, *A&ASS*, 83, 119
 Churchwell E., 2000, in: *Unsolved Problems in Stellar Evolution*, Space Science Library
 Dame T.M. Ungerechts H., Cohen R.S., 1987, *ApJ*, 322, 706
 Danby G., Flower D.R., Valiron P., Schilke P., Walmsley C.M., 1988, *MNRAS*, 235, 229
 Egan M.P., Shipman R.F., Price S.D., Carey S.J., Clark F.O., 1998, *ApJ*, 494, L199
 Fomalont E.B., Windhorst R.A., Fristian J.A., Kellerman K.I., 1991, *AJ*, 102, 125
 Garay G., Rodriguez L.F., Moran J.M., Churchwell E., 1993, *ApJ*, 418, 368
 Garay G., Ramirez S., Rodriguez L.F., Curiel S., Torrelles J.M., 1996, *AJ*, 459, 193
 Gezari D.Y., 1982, *ApJ*, 259, 29
 Gregory P.C., Condon J.J., 1991, *ApJS*, 75, 1011
 Griffith M.R., Wright A.E., Burke B.F., Ekers R.D., 1994, *ApJS*, 90, 179
 Henning T., Klein R., Launhardt R., Schreyer K., Stecklum B., 2000, in: *Infrared Surveys*, Springer Verlag, eds. Lemke D.
 Hillenbrand L., Hartmann L.W., 1998, *ApJ*, 492, 540
 Hofner P., Cesaroni R., Rodriguez L.F., Marti J., 1999, *A&A*, 345, L43
 Hunter T., 1997, Ph.D. Thesis, Caltech
 Hunter T., Neugebauer G., Benford D.J., Matthews K., Lis D.C., Serabyn E., Phillips T.G., 1998, *ApJ*, 493, L97
 Hunter T., Churchwell E., Watson C., Cox P., Benford D.J., Roelfsema P.R., 2000, *ApJ*, accepted
 Jijina J., Myers P.C., Adams F.C., 1999, *ApJS*, 125, 161
 Kreysa E., Gemünd H.P., Gromke J., et al. 1998, *Proc. SPIE*, 3357, 319
 Kuchar T.A., Bania T.M., 1994, *ApJ*, 436, 117
 Kurtz S., Churchwell E., Wood D.O.S., 1994, *ApJ*, 91, 1994
 Kurtz S., Cesaroni R., Churchwell E., Walmsley C.M., 2000, in *Protostars & Planets IV*, ed. V. Mannings
 Lada C., 1993, in: *The Physics of Star Formation and Early Stellar Evolution*, NATO ASI Series, Vol. 342, eds. Lada C., and Kylafis D.
 Lang K., 1992, *Astrophysical Data*, Springer Verlag New York, Inc.
 Lis D.C., Serabyn E., Keene J., Dowell C.D., Benford D.J., Phillips T.G., 1998, *ApJ*, 509, 299
 Marti J., Rodriguez L.F., Torrelles J.M., 1999, *A&A*, 345, L5
 MacLeod G.C., Gaylard M.J., 1992, *MNRAS*, 256, 519
 Mathis J.S., 1990, *ARAA*, pp. 37
 Massey P., 1998, in: *The Stellar Initial Mass function*, ASP Conference Series, Vol. 142, eds Gilmore G. and Howell D.
 McCluskey G.E., Kondo Y., 1972, *Astrophysics and Space Science* 17, pp. 134-149
 Megeath S.T., Tieftrunk A.R., 1999, *ApJ*, 526, L113
 Menten K.M., Reid M.J., 1995, *ApJ*, 445, L157
 Menten K.M., 1996, in *IAU Symposium 178*, ed. E. v. Dishoek
 Menten K.M., Sridharan T.K., Wyrowski F., Schilke P., 1999, in: *The Physics and Chemistry of the Interstellar Medium*, ed. V. Ossenkopf, GCA-Verlag Herdecke
 Mezger P.G., Wink J.E., Zylka R., 1990, *A&A*, 228, 95
 Molinari S., Brand J., Cesaroni R., Palla F., 1996, *A&A*, 308, 573
 Molinari S., Testi L., Brand J., Cesaroni R., Palla F., 1998, *A&A*, 505, L39
 Molinari S., Brand J., Cesaroni R., Palla F., Palumbo G., 1998, *A&A*, 326, 339
 Molinari S., Brand J., Cesaroni R., Palla F., 2000, *A&A*, 355, 617
 Norberg P., Maeder A., 2000, *A&A*, 359, 1025
 Osorio M., Lizano S., D'Alessio P., 1999, *ApJ*, 525, 808
 Palla F., Stahler S., 1993, *ApJ*, 418, 414
 Porras A., Cruz-Gonzales L., Salas L., 2000, *A&A*, in press
 Ramesh B., Sridharan T.K., 1997, *MNRAS*, 284, 1001
 Reid M.J., Argon A.L., Masson C.R., Menten K.M., Moran J.M., 1995, *ApJ*, 443, 238
 Sanders D.B., Clemens D.P., Scoville N.Z., Solomon P.M., 1986, *ApJS*, 60, 1
 Scalo J., 1986, *Fund. Cosmic Phys.*, 11, 1
 Schatzman E., Praderie F., 1993, *The Stars*, Springer Verlag
 Schilke P., Walmsley C., Pineau de Forêts, Flower D., 1997, *A&A*, 321, 293
 Shepherd D.S., Churchwell E., 1996, *ApJ*, 472, 225
 Shepherd D.S., Watson A., Sargent A., Churchwell E., 1998, *ApJ*, 507, 861
 Shepherd D.S., Yu K.C., Bally J., Testi L., 2000, *ApJ*, 535, 833
 Slysh V.I., Val'tts I.E., Kalenski S.V., Voronkov M.A., Palagi F., Tofani G., Catarzi M., 1999, *A&AS*, 134, 115
 Snell R.L., Dickman R.L., Huang Y.-L., 1990, *ApJ*, 352, 139
 Sridharan T.K., Menten K.M., Wyrowski F., Schilke P., 1999, in: *Star Formation 1999*, ed. T. Nakamoto, The Nobeyama Radio Observatory
 Stahler S., Palla F., Ho P., 2000, in *Protostars & Planets IV*, The University of Arizona Press
 Szymczak M., Hrynek G., Kus A., 2000, *A&AS*, 143, 269
 Testi L., talk held at the workshop on massive star formation, Volterra, June 2000
 Tieftrunk A.R., Gaume R.A., Claussen M.J., Wilson T.L., Johnston K.J., 1997, *A&A*, 318, 931
 Ungerechts H., Walmsley M.C., Winnewisser G., 1986, *A&A*, 157, 207
 Walmsley M.C., 1995, *RevMexAA*, 1, 137

Walsh A.J., Hyland A.R., Robinson G., Burton M.G., 1998, MNRAS, 291, 261
 Walsh A.J., Burton M.G., Hyland A.R., Robinson G., 1998, MNRAS, 301, 640
 Walsh A.J., Bertoldi F., Burton M.G., Nikola T., 2001, MNRAS. in press
 Wilking B.A., Mundy L.G., Blackwell J.H., Howe J.E., 1989, ApJ, 345, 257
 van der Walt D.J., Gaylard M., MacLeod G.C., 1995, A&AS, 110, 81
 Wilner, D.J., Welch, W.J., Forster, J.R., 1995, ApJ, 449, L73
 Wolfire M.G. & Cassinelli J.P., 1987, ApJ, 319, 850

Wood, D.O.S., Churchwell, E., 1989, ApJ, 340, 265
 Wood, D.O.S., Churchwell, E., 1989, ApJS, 69, 831
 Wright A.E., Griffith M.R., Burke B.F., Ekers R.D., 1994, ApJS, 91, 111
 Wyrowski F., Schilke P., Walmsley C.M.; Menten K.M., 1999, ApJ, 514, L43
 Zhang Q., Hunter T.R., Sridharan T.K., Cesaroni R., 1999, ApJ, 527, L117
 Zhang Q., Hunter T.R., Brand J., Sridharan T.K., Molinari S., Kramer M., Cesaroni R., 2001, ApJ, accepted
 Zylka R., 1998, Pocket Cookbook for the MOPSI Software, MPIfR internal report

TABLE 1
 THE SAMPLE

source	R.A. [J2000]	Dec. [J2000]	v_{LSR} [km/s]	d_{far} [kpc]	d_{near} [kpc]	T_{cd} [K]	T_{hd} [K]	L_{far} $\log(L_{\odot})$	L_{near} $\log(L_{\odot})$	12/100 [μ]	$T_{\text{rot}}(\text{NH}_3)$ [K]	MSX
05358+3543	05 39 10.4	+35 45 19	-17.6	1.8 ¹		47	100	3.8		60	18	-
05490+2658	05 52 12.9	+26 59 33	0.8	2.1 ¹		44	167	3.5				1
05553+1631	05 58 13.9	+16 32 00	5.7	2.5 ¹		56	114	3.8				1
18089-1732	18 11 51.3	-17 31 29	33.8	13.0	3.6	40	113	5.6	4.5	100	38	4
18090-1832	18 12 01.9	-18 31 56	109.8	10.0	6.6	36	157	4.5	4.1			1
18102-1800	18 13 12.2	-17 59 35	21.1	14.0	2.6	35	161	5.3	3.8		15	1
18151-1208	18 17 57.1	-12 07 22	32.8	3.0		47	170	4.3			17	1
18159-1550	18 18 47.3	-15 48 58	59.9	11.7	4.7	55	123	5.0	4.2			1
18182-1433	18 21 07.9	-14 31 53	59.1	11.8	4.5	43	118	5.1	4.3		20	1
18223-1243	18 25 10.9	-12 42 17	45.5	12.4	3.7	50	173	5.3	4.2		18	1
18247-1147	18 27 31.1	-11 45 56	121.7	9.3	6.7	35	132	5.0	4.8			2
18264-1152	18 29 14.3	-11 50 26	43.6	12.5	3.5	35	151	5.1	4.0		18	1
18272-1217	18 30 02.7	-12 15 27	34.0	2.9		52	181	4.0				1
18290-0924	18 31 44.8	-09 22 09	84.3	10.5	5.3	40	165	5.0	4.4		20	1
18306-0835	18 33 21.8	-08 33 38	76.8	10.7	4.9	34	154	4.8	4.1			1
18308-0841	18 33 31.9	-08 39 17	77.1	10.7	4.9	38	142	4.9	4.2		18	1
18310-0825	18 33 47.2	-08 23 35	84.4	10.4	5.2	40	129	4.8	4.2		18	3
18337-0743	18 36 29.0	-07 40 33	57.9	11.5	4.0	37	139	5.0	4.0		17	1
18345-0641	18 37 16.8	-06 38 32	95.9	9.5 ⁵		36	161	4.6			16	1
18348-0616	18 37 29.0	-06 14 15	109.5	9.0	6.3	39	159	5.1	4.8		19	3
18372-0541	18 39 56.0	-05 38 49	23.6	13.4	1.8	33	204	5.3	3.5	110	16	1
18385-0512	18 41 12.0	-05 09 06	26.0	13.1	2.0	49	157	5.3	3.7			1
18426-0204	18 45 12.8	-02 01 12	15.0	13.5	1.1	32	204	5.0	2.8			1
18431-0312	18 45 46.9	-03 09 24	105.2	8.2	6.7	34	199	4.5	4.4		15	2
18437-0216	18 46 22.7	-02 13 24	110.8	7.3		31	221	4.4				2
18440-0148	18 46 36.3	-01 45 23	97.6	8.3 ⁶		97	121	4.7		75	23	1
18445-0222	18 47 10.8	-02 19 06	86.8	9.4	5.3	45	159	5.2	4.7		21	1
18447-0229	18 47 23.7	-02 25 55	102.6	8.2	6.6	36	172	4.6	4.4		15	1
18454-0136	18 48 03.7	-01 33 23	38.9	11.9	2.7	31	142	4.8	3.5		22	1
18454-0158	18 48 01.3	-01 54 49	52.6	5.6 ⁷		34	170	4.3				3
18460-0307	18 48 39.2	-03 05 53	83.7	9.5 ⁷	5.2	43	176	4.6	4.1		19	3
18470-0044	18 49 36.7	-00 41 05	96.5	8.2 ⁷		56	158	4.9			20	2
18472-0022	18 49 50.7	-00 19 09	49.0	11.1	3.2	49	135	4.9	3.8			1
18488-0000	18 51 24.8	+00 04 19	82.7	8.9	5.4	42	169	4.9	4.5		20	1
18517+0437	18 54 13.8	+04 41 32	43.9	2.9		38	176	4.1				1
18521+0134	18 54 40.8	+01 38 02	76.0	9.0	5.0	37	151	4.6	4.1	90		1
18530+0215	18 55 34.2	+02 19 08	77.7	8.7	5.1	51	127	5.4	4.9		16	1
18540+0220	18 56 35.6	+02 24 54	49.6	10.6	3.3	38	159	4.9	3.9			2
18553+0414	18 57 52.9	+04 18 06	10.0	12.9	0.6	42	152	5.1	2.4			-
18566+0408	18 59 09.9	+04 12 14	85.2	6.7		51	161	4.8			15	1
19012+0536	19 03 45.1	+05 40 40	65.8	8.6	4.6	43	139	4.7	4.2		21	1
19035+0641	19 06 01.1	+06 46 35	32.4	2.2 ⁸		51	100	3.9			21	1
19074+0752	19 09 53.3	+07 57 22	54.8	8.9	3.7	45	144	4.8	4.0		16	1
19175+1357	19 19 49.1	+14 02 46	14.6	10.6 ⁹		36	165	4.8				3
19217+1651	19 23 58.8	+16 57 37	3.5	10.5		38	124	4.9			25	-
19220+1432	19 24 19.7	+14 38 03	68.8	5.5		43	151	4.4			23	1
19266+1745	19 28 54.0	+17 51 56	5.0	10.0	0.3	32	176	4.7	1.7			2
19282+1814	19 30 28.1	+18 20 53	23.6	8.2	1.9	36	231	4.9	3.6			1
19403+2258	19 42 27.2	+23 05 12	26.7	6.3	2.4	57	150	4.7	3.8			1
19410+2336	19 43 11.4	+23 44 06	22.4	6.4	2.1	46	147	5.0	4.0		18	1
19411+2306	19 43 18.1	+23 13 59	29.0	5.8	2.9	41	157	4.3	3.7		14	1
19413+2332	19 43 28.9	+23 40 04	20.8	6.8	1.8	41	133	4.4	3.3		18	1
19471+2641	19 49 09.9	+26 48 52	21.0	2.4 ¹⁰		38	194	3.6		130		2
20051+3435	20 07 03.8	+34 44 35	11.6	3.7	1.6	49	143	4.0	3.3			1
20081+2720	20 10 11.5	+27 29 06	5.7	0.7 ²		34	248	2.5				1
20126+4104	20 14 26.0	+41 13 32	-3.8	1.7 ²		62	112	3.9			23	1
20205+3948	20 22 21.9	+39 58 05	-1.7	4.5		48	175	4.5				1
20216+4107	20 23 23.8	+41 17 40	-2.0	1.7 ²		46	159	3.3			21	1
20293+3952	20 31 10.7	+40 03 10	6.3	2.0	1.3	56	157	3.8	3.4		15	1
20319+3958	20 33 49.3	+40 08 45	8.8	1.6		73	162	3.8				-
20332+4124	20 35 00.5	+41 34 48	-2.0	3.9		56	148	4.8			17	-
20343+4129	20 36 07.1	+41 40 01	11.5	1.4		44	150	3.5			18	-
22134+5834	22 15 09.1	+58 49 09	-18.3	2.6		61	135	4.1			18	-
22551+6221	22 57 05.2	+62 37 44	-13.4	0.7 ³		45	186	3.2				-
22570+5912	22 59 06.5	+59 28 28	-46.7	5.1		54	145	4.7				-
23033+5951	23 05 25.7	+60 08 08	-53.1	3.5 ⁴		52	149	4.0			20	1
23139+5939	23 16 09.3	+59 55 23	-44.7	4.8		41	140	4.4				1
23151+5912	23 17 21.0	+59 28 49	-54.4	5.7		68	175	5.0				1
23545+6508	23 57 05.2	+65 25 11	-18.4	0.8 ²		50	181	3.0			18	1

Note. — Only far and no near distance means that the distance ambiguity is solved. Rotation temperatures $T_{\text{rot}}(\text{NH}_3)$ are correct to approximately 3 K. The 12/100 column refers to offsets between the corresponding IRAS sources and the last column shows the number of MSX point source catalog detections in fields of radius $2'$ around the IRAS position. ¹ Snell et al. 1990; ² Wilking et al. 1989; ³ Blaauw 1964; ⁴ Jijina et al. 1999; ⁵ Garay et al. 1993; ⁶ Walsh et al. 1997; ⁷ Kuchar & Bania 1994; ⁸ Osterloh et al. 1996; ⁹ near star HD231160; ¹⁰ near star CGO 544

TABLE 2
OBSERVING PARAMETERS

	freq.	HPBW	T_{sys}	Δv	Obs.	tracer
	[GHz]	[$''$]	[K]	[km s^{-1}]		
$^{12}\text{CO } 2 \rightarrow 1$	230.5	11	250	0.1	PV	outflow
$\text{SiO } 2 \rightarrow 1$	86.9	29	85	3	PV	outflow
$\text{H}^{13}\text{CO}^+ 1 \rightarrow 0$	86.9	29	85	3	PV	dense core
$^{13}\text{CO } 1 \rightarrow 0$	110.2	22	120	0.8	PV	dense core
$\text{CH}_3\text{OH } J_k = 5_k \rightarrow 4_k$	~ 241.8	11	250	0.1	PV	dense core
$\text{CH}_3\text{CN } J = 6 \rightarrow 5$	~ 110.4	22	120	0.8	PV	dense core
$^{12}\text{CO } 2 \rightarrow 1$	230.5	27	500	0.06	CSO	outflow
$\text{NH}_3 (1,1), (2,2)$	~ 22.6	40	50	0.25	Eff.	dense core
$\text{H}_2\text{O maser}$	22.2	40	50	0.03	Eff.	outflow and/or disk ?
$\text{CH}_3\text{OH maser}$	6.7	130	50	0.1	Eff.	high-mass signpost

Note. — Observatories: Eff.: Effelsberg, PV: Pico veleta, CSO: Caltech Submillimeter observatory

TABLE 3
RESULTS

source	cm flux [mJy]	H_2O [Jy]	CH_3OH [Jy]	MSX/cm [$''$]	MSX/mm [$''$]	cm/mm [$''$]	wings	SiO	CH_3OH	CH_3CN
05358+3543	< 1	45	162.0 ¹	—	—	—	+	+	+	—
05490+2658	< 1	—	—	—	16.9	—	+	—	—	—
05553+1631	1.3	—	—	3.5	0.8	2.8	+	+	+	+
18089-1732	0.9	75	54.0 ²	8.1	11.2	3.2	+	+	+	+
18090-1832	?	—	82.0 ²	—	2.6	—	+	—	—	—
18102-1800	44	—	8.8 ³	1.7	25.3	27.0	+	+	—	—
18151-1208	< 1	0.8*	50.0 ⁴	—	8.3	—	+	+	+	+
18159-1550	10.0	?	—	4.4	16.9	12.6	+	—	—	—
18182-1433	< 1	18	24.0 ²	—	10.8	—	+	+	+	+
18223-1243	< 1	—	—	—	3.6	—	+	—	—	—
18247-1147	47	—	1.6	7.4	5.4	1.9	+	—	—	—
18264-1152	< 1	50*	3.8 ¹	—	9.4	—	+	+	+	+
18272-1217	110	—	—	4.4	8.9	5.3	—	—	—	—
18290-0924	7.0	4	15.1 ²	—	12.7	4.5	+	—	—	—
18306-0835	82	0.7*	—	15.5	11.6	11.8	+	—	—	—
18308-0841	< 1	1.5*	—	—	10.6	—	+	+	—	+
18310-0825	7.0	—	—	5.1	16.8	10.6	+	—	—	—
18337-0743	< 1	—	—	—	4.7	—	?	—	—	—
18345-0641	27	3*	5.4 ⁴	—	4.0	—	+	+	+	+
18348-0616	54	—	—	14.8	18.6	67.5	+	—	—	—
18372-0541	80	1.5*	9.2 ¹	3.0	1.8	1.9	+	—	—	—
18385-0512	29	200	—	4.4	2.8	3.4	+	—	—	—
18426-0204	1.6	?	1.3	6.7	12.0	17.6	+	—	—	—
18431-0312	3.5	—	—	30.3	2.4	32.0	+	—	—	—
18437-0216	< 1	—	—	—	6.9	—	?	—	—	—
18440-0148	< 1	?	4.0 ²	—	2.6	—	+	—	—	—
18445-0222	68	—	—	0.4	18.5	18.9	?	—	—	—
18447-0229	1.6	—	—	13.2	4.4	10.0	?	—	—	—
18454-0136	42	—	2.5 ¹	—	4.6	6.7	+	—	—	—
18454-0158	18	—	—	—	2.2	—	+	—	—	—
18460-0307	< 1	—	—	—	5.3	—	+	—	—	—
18470-0044	?	—	7.5 ³	—	20.6	—	+	+	+	+
18472-0022	110	—	—	—	2.1	0.8	+	—	—	—
18488+0000	194	1*	16.9 ⁴	19.0	4.1	16.2	+	+	+	+
18517+0437	< 1	45.3	279 ¹	—	22.6	—	+	—	—	—
18521+0134	< 1	—	1.3	—	3.7	—	+	—	—	—
18530+0215	311	—	—	7.3	7.2	3.8	+	+	+	+
18540+0220	97	—	—	12.1	2.8	10.3	?	—	—	—
18553+0414	< 1	50*	—	—	—	—	+	—	—	—
18566+0408	< 1	3*	7.2 ³	—	0.9	—	+	+	+	+
19012+0536	< 1	2*	0.9	—	5.9	—	+	+	+	—
19035+0641	4.0	9	14.3 ⁵	5.1	7.1	9.0	+	+	+	—
19074+0752	14.8	—	—	—	2.3	—	+	—	—	—
19175+1357	5.1	—	—	—	2.1	37.0	+	—	—	—
19217+1651	32	9*	0.9	—	6.5	—	+	+	+	+
19220+1432	11.0	—	—	4.8	6.1	10.4	+	—	—	—
19266+1745	< 1	1.5*	1.7 ¹	—	4.1	—	+	—	—	—
19282+1814	< 1	—	2.9 ¹	—	11.8	—	+	—	—	—
19403+2258	< 1	—	—	—	23.5	—	+	—	—	—
19410+2336	1.0	110	30.0 ¹	—	3.8	—	+	+	+	+
19411+2306	< 1	—	—	—	2.5	—	+	+	+	—
19413+2332	< 1	—	—	—	11.1	—	+	+	+	—
19471+2641	?	—	—	—	—	—	+	—	—	—
20051+3435	< 1	—	—	—	6.7	—	+	—	—	—
20081+2720	< 1	—	—	—	—	—	+	—	—	—
20126+4104	?	15	36.0 ⁶	—	2.6	—	+	+	+	+
20205+3948	8.3	—	—	12.1	11.5	23.0	+	—	—	—
20216+4107	1.4	—	—	—	4.3	—	+	—	—	—
20293+3952	7.6	100*	—	2.0	23.5	15.0	+	+	+	+
20319+3958	25	—	—	8.3	8.5	15.5	+	—	—	—
20332+4124	136	0.6*	—	—	10.5	—	+	—	—	—
20343+4129	1.8	—	—	—	13.2	—	+	—	—	—
22134+5834	3.7	—	—	—	3.5	—	+	—	—	—
22551+6221	4.5	—	—	—	74.7	—	+	—	—	—
22570+5912	29	—	—	6.4	13.3	7.3	+	—	—	—
23033+5951	1.7	4	—	—	10.6	7.2	+	+	+	—
23139+5939	1.4	400	2.6 ¹	2.1	1.2	1.0	+	+	+	+
23151+5912	< 1	60	—	—	7.7	—	+	+	—	—
23545+6508	1.0	—	—	13.0	26.3	24.2	+	+	—	—

Note. — *: new detections, ??: tentative detections; the MSX/cm MSX/mm and cm/mm columns present offsets between the different observations, and the last 4 column show detections (+), non-detection (−) or non-observations (empty space); ¹ Szymczak et al. 2000; ² Walsh et al. 1998; ³ Slysh et al. 1999; ⁴ v. d. Walt et al. 1995; ⁵ Caswell Vaile 1995; ⁶ MacLeod 1992

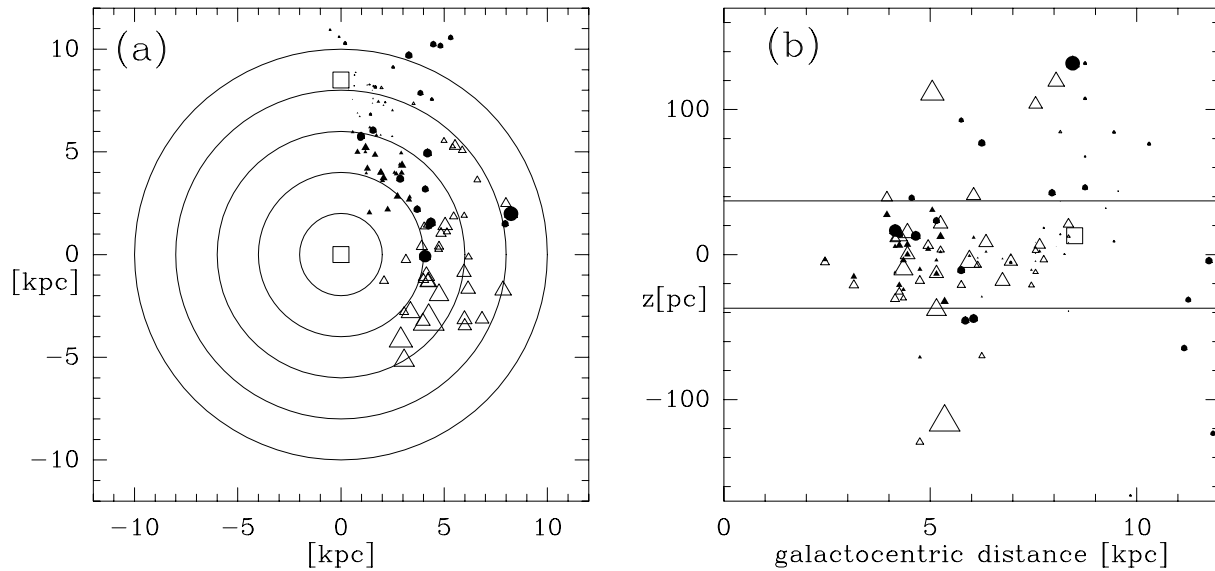


FIG. 1.— **(a)** The Galactic distribution of the sample: filled circles represent sources with no distance ambiguity, triangles show sources with distance ambiguities (filled triangles: near; open triangles: far). The size of the symbols scales with their luminosity. Squares show the Galactic center and the location of the sun (8.5 kpc from the center), while the circles indicate galactocentric distances in 2 kpc steps. **(b)** The Galactic scale height distribution of the sample. Symbols are the same as in (a). The horizontal lines show the average Galactic scale height of massive star formation regions 37 pc (Bronfman et al. 2000).

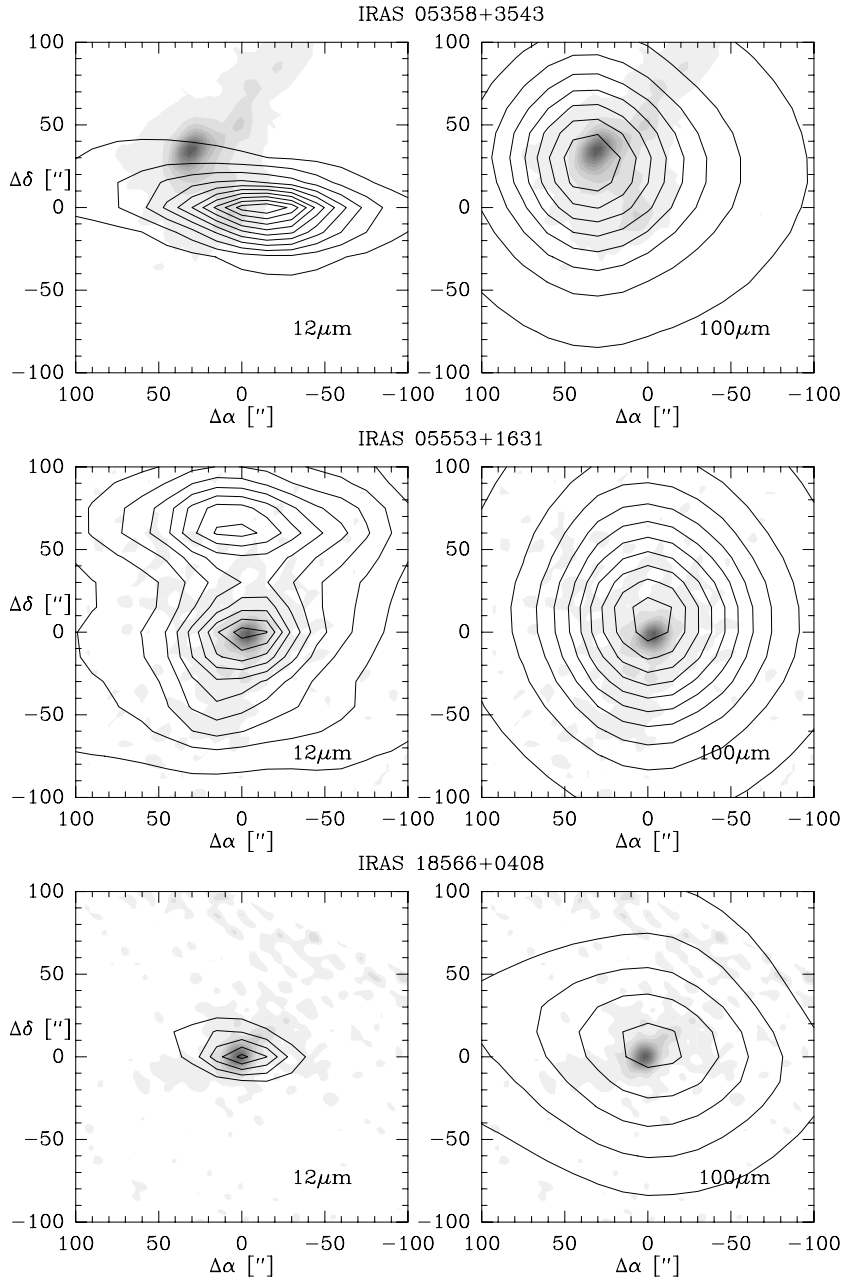


FIG. 2.— Examples of the HIRES images (contours) at 12 μ m and 100 μ m on greyscale 1.2 mm dust images (Beuther et al. 2001). While the bottom images are typical with both HIRES bands corresponding to the same mm core, the middle and top images are counterexamples with the 12 μ m peaks splitting up or tracing different sources in the same field of view.

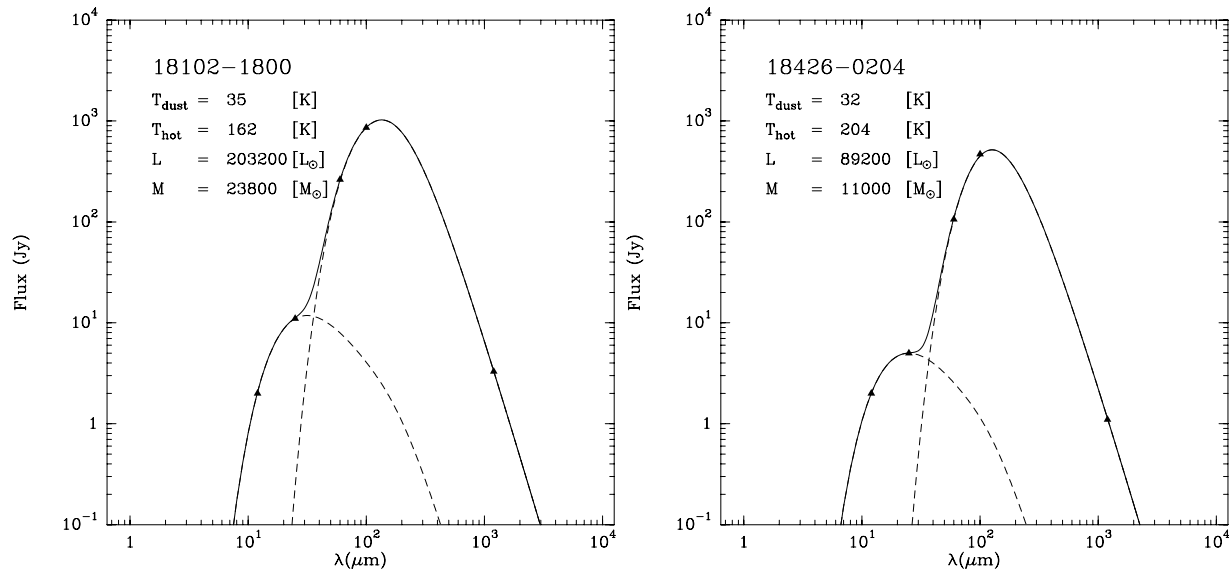


FIG. 3.— Examples of HIRES 2 component greybody fits. While the dashed lines show the two greybodies separately, the full line shows the two component fit. Each panel presents on the top left the source name, luminosities and temperatures.

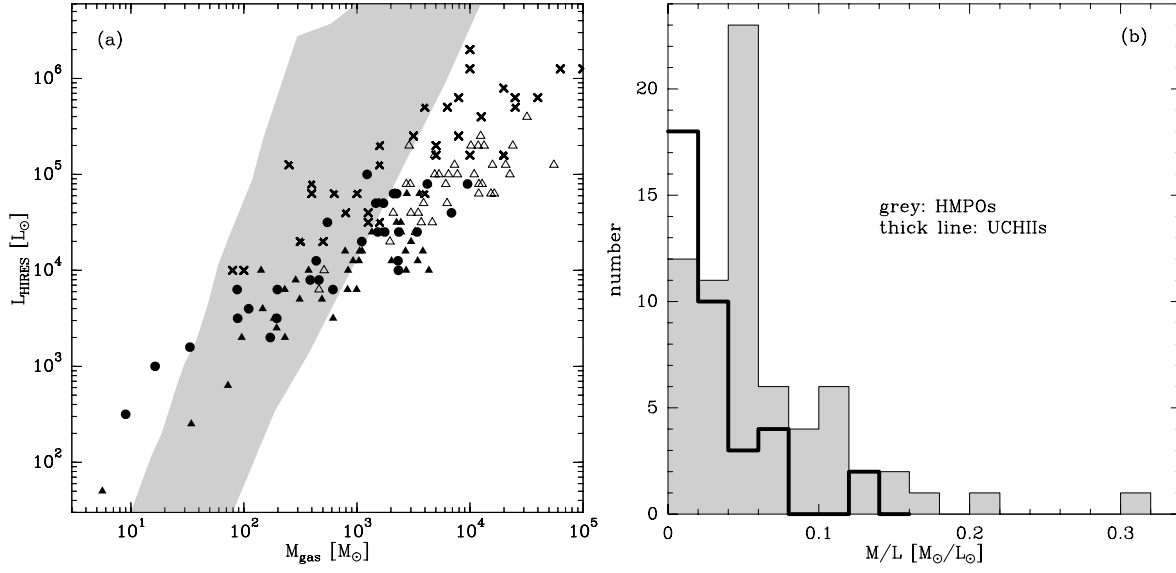


FIG. 4.— **(a)**: Plotted are the derived FIR luminosities against the core masses. Triangles show HMPOs with distance ambiguity (filled: near distance; open: far distance) and filled circles without distance ambiguity. The crosses show data from UCHII regions (Hunter et al. 1997, 2000). The grey shaded area defines the region in which 90% of the simulated clusters are found (Walsh et al. 2001). **(b)**: The histogram presents the distance independent quantity M/L with again a clear separation of HMPOs (grey) and UCHIIs (thick line).

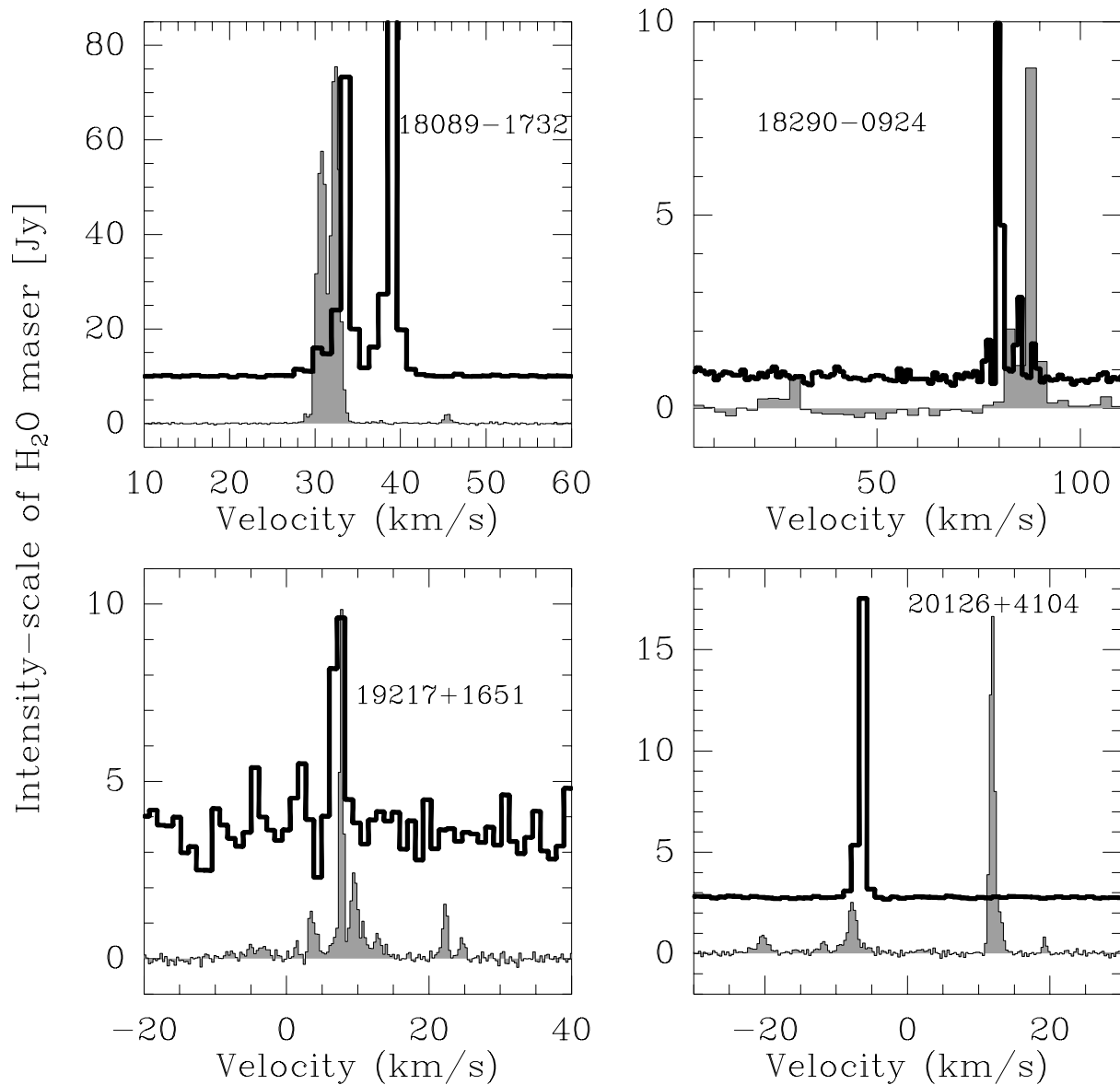


FIG. 5.— Water (grey shaded) and methanol (thick lines) maser example spectra. The abscissa shows the velocities (LSR) for both spectra, while the ordinate shows the intensity of the water maser in [Jy], the methanol maser intensity is shown in arbitrary units.

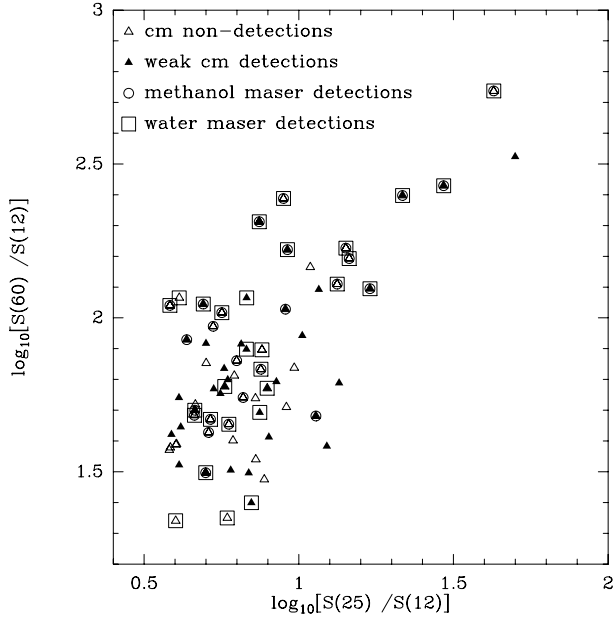


FIG. 6.— *IRAS* Color-color diagram of the whole sample: open triangles represent sources without and filled triangles with cm emission. The surrounding circles and squares represent detected methanol and water maser emission, respectively

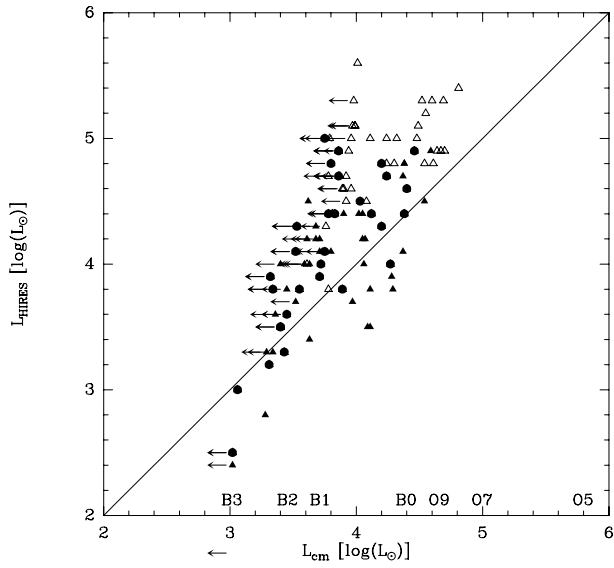


FIG. 7.— The HIRES IR luminosities are plotted against the luminosities based on the cm observations. Again filled circles show sources with no distance ambiguities and triangles sources with distance ambiguities (filled: near distance; open: far distance) The straight line shows the 1:1 correlation.